Thota, P., Krauskopf, B., & Lowenberg, M. H. (2008). Interaction of torsion and lateral bending in aircraft nose landing gear shimmy.

manuscript No.
(will be inserted by the editor)

Interaction of torsion and lateral bending in aircraft nose landing gear shimmy

Phanikrishna Thota[1], Bernd Krauskopf[1] and Mark Lowenberg[2]

[1] Department of Engineering Mathematics, University of Bristol, Queen's Building, University Walk, Bristol BS8 1TR, United Kingdom
[2] Department of Aerospace Engineering, University of Bristol, Queen's Building, University Walk, Bristol BS8 1TR, United Kingdom

The date of receipt and acceptance will be inserted by the editor

Abstract In this paper we consider the onset of shimmy oscillations of an aircraft nose landing gear. To this end we develop and study a mathematical model with torsional and lateral bending modes that are coupled through a wheel-mounted elastic tyre. The geometric effects of a positive rake angle are fully incorporated into the resulting five-dimensional ordinary differential equation model. A bifurcation analysis in terms of the forward velocity and the vertical force on the gear reveals routes to different types of shimmy oscillations. In particular, we find regions of stable quasiperiodic shimmy where both modes are fully excited.

Key words aircraft dynamics – shimmy oscillations – mode interaction – quasiperiodic motion

1 Introduction

Lateral, unwanted oscillations during the motion of wheeled vehicles such as aircraft, motorcycles, cars and trailers are undesirable due to their detrimental effects on the safety as well as on the costs involved in the maintenance of the vehicle. Such oscillations are generally referred to as *shimmy oscillations*. One of the earliest documented evidence of shimmy was reported by Broulhiet [3], who investigated the dynamics of cars. The concept of side slip that he introduced still forms the basis for the understanding of shimmy in a wide range of wheeled vehicles. Another milestone for shimmy research was the seminal work of von Schlippe and Dietrich [17] on tyre mechanics and its influence on shimmy. Shimmy has been studied in general wheeled vehicles, including cars, pulled trailers, motorcycles and aircraft; see, for example, the overview papers by Dengler *et al.* [4], Smiley [13] and Pritchard [12] as an entry point to the literature.

Of particular interest for our study is the work by Pacejka [11] and by Stépán [15, 16], who consider a pulled trailer — a system that is characterized by a large caster length (mechanical trail) with zero rake angle and weak damping, and possible free-play at the kingpin. Pacejka [11] found experimentally and in a 13th-order model that shimmy may occur for a wide range of velocities and may be associated with sudden jumps into and out of shimmy when the velocity is changed. Furthermore, he found the first example of quasiperiodic shimmy in the form of beating oscillations where also the translational mode at the kingpin is excited. Sudden jumps from straight-line motion (no shimmy) of the tyre to large amplitude shimmy with

only a very small variation in the system parameter were also found by Stépán [16]. Furthermore, in [15] he systematically investigates quasiperiodic shimmy oscillations and shows that in his pulled trailer setup the second frequency is due to a memory effect associated with the rolling tyre. This type of tyre dynamics must be modelled mathematically by a set of time-delayed differential equations. In separate work, Takács and Stépán [18] found quasiperiodic shimmy in an experimental setup resembling a pulled trailer; the experimental observations are also verified by comparison with a time-delayed mathematical model.

In this paper we consider the onset of shimmy for the case of an aircraft nose landing gear — an issue that is essentially as old as aircraft themselves. While there are certain commonalities, there are important differences between different types of vehicles, which are crucial for the dynamics and the onset of shimmy. The nose landing gear of a typical mid-size commercial passenger aircraft has three main vibrational modes: a torsional mode corresponding to the rotation about the strut axis, a lateral mode that is representative of vibrations of the gear about an axis passing through the fuselage centreline, and a vertical mode associated with the shock dampers (oleos) of the gear. These three modes of vibration are coupled via the tyre-ground interaction and play an important role in the occurrence of shimmy in aircraft. In contrast to pulled trailers, an aircraft nose landing gear generally features a non-zero rake angle and its torsional mode is very strongly damped.

Initial work in the early 1930s on the dynamic stability of aircraft on the ground concentrated on the excitation of the vertical mode via roughness of the ground. See the overview paper by Dengler *et al.* [4] for a discussion of the early literature on how the vertical mode may interact with either the torsional or with the lateral mode. By contrast, the vertical mode of a commercial aircraft is generally sufficiently damped so that it does not get excited on today's smooth runways or taxiways. Nevertheless, shimmy may still occur in aircraft landing gears, and this has been studied experimentally, by means of linear stability analysis and by numerical simulation; see the reviews [1,2,6,8]. Smiley [13] studied shimmy for three different landing gear structures. While one of the cases had a non-zero rake angle, its nonlinear geometric effects were not included in the model. The paper [13] contains linear stability analysis of a landing gear model and discusses a systematic way of modeling the geometrical aspects of the strut. More recently, Somieski [14] studied shimmy as a nonlinear phenomenon for a nonlinear set of ODEs describing a nose landing gear with zero rake angle. Here, time domain analysis showed a case of supercritical Hopf bifurcation leading to a set of stable limit cycles past the bifurcation point. Woerner and Noel [21] describe the main cause of shimmy as the energy transfer from the contact force between the tyres and the ground to the vibrational modes of the landing gear system whose stability depends on the damping and stiffness characteristics of tyres and the supporting structure. They also studied the change in the frequency of different vibrational modes of a typical nose landing gear as a function of swivel friction and forward velocity. This suggests that coupled motion can occur due to resonance phenomena under variations in the forward velocity leading to high-amplitude shimmy oscillations.

The focus of this work is the interaction between the torsional mode and the lateral mode, which are strongly coupled via the nonlinear restoring force of the elastic tyre. Specifically, we develop a mathematical model in the form of a five-dimensional system of ordinary differential equations for the two modes and the kinematic equation of the nonlinear tyre. Here we use a variant of the widely accepted *stretched string* model developed by von Schlippe [17], where we include the effect of lateral bending on the lateral deformation of the tyre. Importantly, we include in the model the geometric effects of a non-zero rake angle of the gear.

A bifurcation analysis of our mathematical model with the software package AUTO [5] reveals a two-parameter bifurcation diagram in the plane of forward ve-

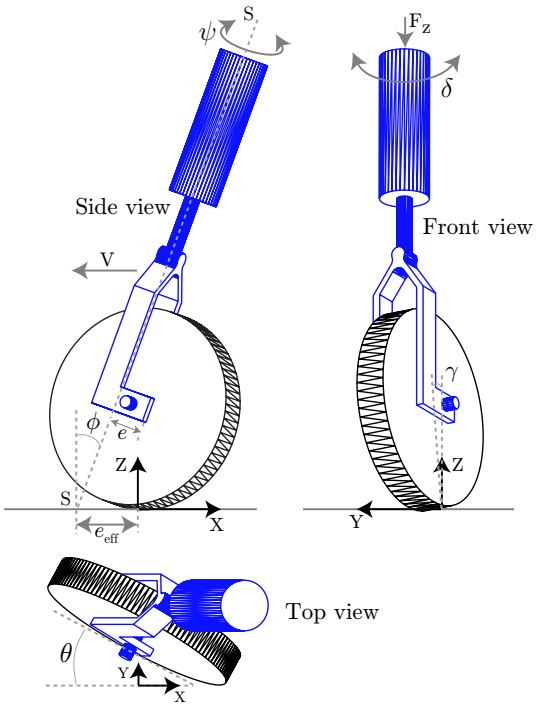

Figure 1 Schematic side, front and top views of an aircraft nose landing gear.

locity and vertical force on the gear. The main features of the bifurcation diagram are two curves of Hopf bifurcations, of the torsional mode and the lateral mode, respectively, which intersect at two double Hopf points. These codimension-two points give rise to curves of torus bifurcations that are associated with the emergence of quasiperiodic shimmy oscillations. Overall, we find a comprehensive picture of parameter regions corresponding to stable straight-line motion, torsional, lateral and quasiperiodic shimmy oscillations.

The paper is organized as follows. In Sec. 2 we develop the mathematical model, which involves deriving the relevant coupling terms between the torsional and lateral modes via nonlinear tyre forces. Section 3 is devoted to the bifurcation analysis of the model. We first show selected one-parameter continuations in the forward velocity and then present the bifurcation diagram in the plane of forward velocity and vertical force on the gear; representative time series of different types of shimmy are also presented. Section 4 summarizes and discusses directions of future research.

2 Model of a nose landing gear with torsional and lateral dynamics

The nose landing gear of an aircraft consists of a strut that is attached to the aircraft fuselage and coupled to the ground via one or more wheels with flexible tyres. We consider here a nose landing gear as sketched in Fig. 1. Throughout this work we use one of the conventionally accepted coordinate systems for aircraft analysis. Specifically, the positive X-axis points towards the backward direction of the aircraft, the Z-axis is the upward normal to the (flat) ground, and the Y-axis completes the right-handed coordinate system.

The strut is able to rotate about its axis S, which gives rise to a steering angle ψ. The wheel axle, offset from the strut axis by a mechanical trail (caster) of length e, supports a wheel with tyre of radius R. Importantly, the strut axis is inclined to the vertical at a rake angle ϕ. The aircraft body is modeled as a block of mass exerting

Table 1 System parameters and their values as used in the modeling.

symbol	parameter	value	
	structure parameters		
e	caster length	0.12	m
l_g	gear height	2.5	m
k_ψ	torsional stiffness of strut	$-1.0\text{x}10^5$	N m rad^{-1}
c_ψ	torsional damping of strut	-45.0	N m s rad^{-1}
I_z	moment of inertia of strut w.r.t z-axis	1.0	kg m^2
k_δ	lateral bending stiffness of strut	$-3.35\text{x}10^7$	N m rad^{-1}
c_δ	lateral bending damping of strut	-150.0	N m s rad^{-1}
I_x	moment of inertia of strut w.r.t x-axis	1.0	kg m^2
ϕ	rake angle	0.1571	rad (9^o)
	tyre parameters		
R	radius of nose wheel	0.362	m
h	contact patch length	0.1	m
c_λ	damping coefficient of elastic tyre	-270.0	N m^{2}rad^{-1}
k_α	self-aligning coefficient of elastic tyre	-2.0	m/rad
k_λ	restoring coefficient of elastic tyre	20.0	rad^{-1}
L	relaxation length	0.3	m
α_m	self-aligning moment limit	0.1745	rad (10^o)
	continuation parameters		
F_z	vertical force on the gear	10.0-70.0	kN
V	forward velocity	10.0-350	m s^{-1}

a vertical force F_z on the gear, which is moving at a fixed horizontal velocity V. Apart from torsional motion as described by the steering angle ψ, we also consider lateral bending motion of the gear assembly about the Y-axis. The lateral motion is modeled (in first order approximations) by an angle δ that the strut makes with the zero position. These two geometrical degrees of freedom are coupled via the lateral deformation λ of the tyre. The wheel-ground interaction is modeled by the well-established stretched string model from [17] of an elastic tyre, which we modified to incorporate the deformation due to lateral bending mode.

The structure shown in Fig. 1 closely resembles the nose landing gear of an aircraft, which is characterized by a moderate rake angle (about 10 degrees), a small caster length e (about 0.1 m for a mid-size passenger aircraft), and large torsional and lateral bending stiffness and damping due to the steering mechanism. Specifically, we use throughout realistic parameters for geometry and tyre taken from [14] and summarized in Table 1. For comparison, motorcycles generally have large rake angles (possibly even larger than 30 degrees) and a small caster length, while trailers have zero rake angle and a long caster length (up to several metres). Importantly, both motorcycles and trailers generally have very low torsional damping.

The presence of a non-zero rake angle ϕ is incorporated into our model because it has several important geometrical effects in an aircraft nose landing gear. First, it induces an effective caster length e_{eff} [20], which is given by

$$e_{\text{eff}} = e\cos\phi + R\tan\phi + e\sin\phi\tan\phi. \tag{1}$$

Secondly, for a non-zero rake angle the swivel angle θ of the wheel with the ground is different from the steering angle ψ; namely, it is given by $\theta = \psi\ \cos\phi$. Thirdly, there is a tilt $\gamma = \psi\sin\phi$ of the wheel when the steering angle ψ is non-zero. The tilt γ contributes to the overall tilt of the wheel due to lateral bending motion as expressed by δ and both result in a lateral restoring force on the tyre. The point of application of this restoring force is ahead of the centre of the contact patch. Depending on the tilt direction, this lateral tilt force may act in the same or in the

opposite direction of the lateral restoring force created due to pure lateral distortion or torsional motion of the tyre. This can lead to an increase or decrease of the effective self-aligning moment responsible for stabilizing the shimmy oscillations. Since this force is known to affect dynamics of motorcycles and cars **more** than aircraft tyres, we do not consider this force in the analysis.

Another effect of a non-zero rake angle is the increase in the moment that destabilizes the orientation of the gear. The vertical force F_z is offset from the (x-z) plane due to the effective caster length e_{eff}. This offset vertical force generates a moment, increased by the effect of the caster length, and acts to turn the gear about its strut axis. In the case of aircraft landing gears, the high torsional stiffness and damping about the strut axis resist this destabilizing moment. However, in the case of bicycles and motorcycles torsional stiffness and damping are negligibly small, so that this moment makes it very difficult to ride a bike when the handle bar is rotated by 180 degrees.

Taking into account torsional and lateral motion and their coupling through the elastic tyre, the equations for the landing gear model can be written in the form

$$I_z\ \ddot{\psi} = M_{K_\psi} + M_{D_\psi} + M_{F_1} + M_{D_\lambda} + F_z\ \sin(\phi)\ e_{\text{eff}}\ \sin(\theta), \tag{2}$$

$$I_x\ \ddot{\delta} = M_{K_\delta} + M_{D_\delta} + M_{\lambda_\delta} + F_z\ e_{\text{eff}}\ \sin(\theta), \tag{3}$$

$$\dot{\lambda}_A + \frac{V}{L}\lambda_A = V\ \sin(\theta) + l_g\ \dot{\delta}\ \cos(\delta) + (e_{\text{eff}} - h)\ \cos(\theta)\ \dot{\psi}\ \cos(\phi)\,. \tag{4}$$

Equation (2) governs the torsional dynamics and Eq. (3) the lateral dynamics. Equation (4) comes from von Schlippe's stretched string model [17]; it describes the nonlinear kinematic relationship between the steering angle ψ, lateral bending angle δ and the lateral deformation λ_A of the leading edge of the contact patch of the tyre. We now present a detailed description of the individual terms in Eqs. (2)–(4) in the next sections.

2.1 Torsional mode of the landing gear

Equation (2) describes the torsional aspect of the landing gear dynamics. The moment M_{K_ψ} due to the torsional stiffness of the strut is a function of the steering angle ψ and is given by

$$M_{K_\psi} = k_\psi\ \psi, \tag{5}$$

and the moment M_{D_ψ} due to the torsional damping of the strut is a function of the angular velocity of the steering $\dot{\psi}$ and is given by

$$M_{D_\psi} = c_\psi\ \dot{\psi}, \tag{6}$$

where k_ψ and c_ψ are the torsional stiffness and damping coefficients of the strut, respectively. The last three terms in Eq. (2) model the tyre interaction with the ground. Specifically, the combined moment M_{F_1} due to the tyre's restoring force F_{K_λ} and self-aligning moment M_{K_α}, which are functions of the tyre's lateral deformation λ, is given by

$$M_{F_1} = M_{K_\alpha} - e_{\text{eff}}\ F_{K_\lambda}\,. \tag{7}$$

The self-aligning moment M_{K_α} is given by the piecewise continuous function [14]

$$M_{K_\alpha} = \begin{cases} k_\alpha \sin\left(\alpha \frac{\pi}{\alpha_m}\right)\ F_z & \text{if } |\alpha| \le \alpha_m, \\ 0 & \text{if } |\alpha| > \alpha_m, \end{cases} \tag{8}$$

and the lateral restoring force F_{K_λ} due to tyre deformation is given by

$$F_{K_\lambda} = 3.0\ \tan^{-1}(7.0\ \tan(\alpha))\ \cos\left(0.95\ \tan^{-1}(7.0\ \tan(\alpha))\right)\ F_z. \tag{9}$$

Here, k_α and k_λ are the torsional and lateral stiffnesses of the tyre. The slip angle α is related to the lateral deformation λ_A by $\alpha = \tan^{-1}(\lambda_A/L)$, where L is the *relaxation length* of the tyre. The rake angle ϕ enters into the model via the effective caster length as given in (1); note that $e_{\text{eff}} = e$ for $\phi = 0$. The constant α_m is the limit on the slip angle α beyond which the self-aligning moment is taken to be zero.

Finally, in Eq. (2), the moment M_{D_λ} due to the tyre's tread damping is given by

$$M_{D_\lambda} = c_\lambda\ e_{\text{eff}}\ \dot{\lambda}, \tag{10}$$

where c_λ is the lateral damping coefficient of the tyre. For an aircraft nose landing gear, the restoring force generated due to the tilting of the wheel is of the same order of magnitude as the lateral deformation force of the tyre and, hence, tilting moments become important for the shimmy analysis.

2.2 Lateral bending mode of the landing gear

Equation (3) describes the lateral bending motion of the landing gear assembly about the X-axis. The moment M_{K_δ} due to the stiffness of the strut acting against the lateral bending motion is a function of δ and is given as

$$M_{K_\delta} = k_\delta\ \delta, \tag{11}$$

where k_δ is the bending stiffness of the strut w.r.t the rotation about the X-axis.

The moment M_{D_δ} due to the damping characteristics of the strut against the lateral motion is a function of $\dot{\delta}$ and is given as

$$M_{D_\delta} = c_\delta\ \dot{\delta}, \tag{12}$$

where c_δ is the damping coefficient of the lateral bending of the strut. The last two terms in Eq. (3) are contributions of the tyre forces to the bending motion δ. Specifically, the moment M_{λ_δ} is the result of the force created from the lateral deformation of the tyre and is given as

$$M_{\lambda_\delta} = (l_g)\ F_{K_\lambda}\ \cos(\theta)\ \cos(\phi), \tag{13}$$

where l_g is the distance between the point of attachment of the gear to the fuselage and the ground.

2.3 Tyre kinematics

Equation (4) describes the motion of the tyre under the influence of the strut's torsional and lateral bending. Here the effect of the deformation resulting from the lateral bending mode is incorporated into the conventional kinematic equation representing the stretched string theory of a tyre [17]. This is important because the natural frequencies of the lateral and torsional modes are typically different and the resultant lateral deformation is an algebraic sum of the deformation caused by both the modes.

From [17], the nonlinear form of the equation describing the kinematics is given as

$$\dot{\lambda}_A + \frac{V}{L}\lambda_A = V\ \sin(\theta) + (e_{\text{eff}} - h)\ \cos(\theta)\ \dot{\theta}. \tag{14}$$

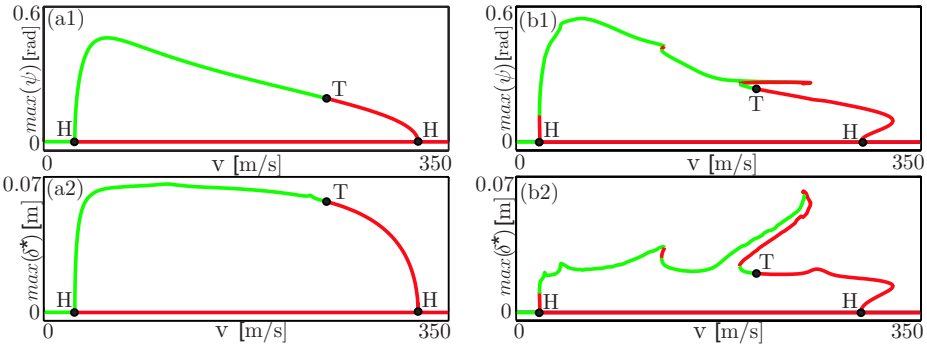

Figure 2 One-parameter continuation in V for $F_z = 20.0\,\text{kN}$ (a) and $F_z = 40.0\,\text{kN}$ (b); the top panels show the maximum of the torsion angle ψ and the bottom panels the maximum of the bending stroke δ^*. Stable parts of branches are green and unstable parts red, with Hopf bifurcations labelled H and torus bifurcations T.

The effect of lateral deformation due to lateral bending on the tyre kinematics can be derived in a similar fashion as in the case of pure torsional mode. Namely, the relationship between the lateral bending angle δ and the lateral deformation λ_A of the tyre at the leading edge of the contact patch is given by:

$$\dot{\lambda}_A + \frac{V}{L}\lambda_A = (l_g)\ \dot{\delta}\ \cos(\delta). \tag{15}$$

Combining Eqs. (14) and (15) yields the kinematic equation (4).

3 Bifurcation analysis

We now perform a bifurcation analysis of the nose landing gear model given by Eqs. (2)–(4) with the continuation software AUTO [5]. Specifically, we consider the dependence of the dynamics on the forward velocity V and the vertical force F_z, where we fix all other system parameter at the realistic values given in Table 1. Our starting point is the transition to shimmy with varying V, which can be studied by means of one-parameter bifurcation diagrams. We then consider the bifurcation diagram in the (V, F_z)-plane to provide a more global view of the overall dynamics. Representative time histories are presented to discuss the possible motion of the nose landing gear in terms of the contributions of torsion and lateral bending.

3.1 Dynamics as a function of forward velocity

Equations (2)–(4) always have the equilibrium solution $(\psi, \delta, \lambda_A) = (0, 0, 0)$, which corresponds to straight-line rolling of the tyre. This equilibrium is stable when the forward velocity V is very low, but as the forward velocity is increased it may lose its stability in a Hopf bifurcation resulting in shimmy oscillations. A continuation in V reveals not only the onset of shimmy, but is also able to follow the ensuing shimmy oscillations to study their stability.

Figure 2 shows two continuations in V for different values of the vertical force F_z; all other parameters are as in Table 1. For $F_z = 20.0\,\text{kN}$ the stable equilibrium becomes unstable in a Hopf bifurcation H at $V \approx 26.9$ m/s. This Hopf bifurcation is supercritical and gives birth to a stable periodic orbit corresponding to shimmy oscillations. It is represented in panel (a1) in terms of the maximum of the torsion angle ψ, and in panel (a2) in terms of the maximum of the lateral bending stroke

$\delta^* = l_g \sin(\delta)$ (at ground level). The onset of shimmy for $F_z = 20.0\,\text{kN}$ in a supercritical Hopf bifurcation is what one finds for models that only feature a torsional mode and no lateral bending [20]. Importantly, without the lateral degree-of-freedom the shimmy oscillations vanish again in another supercritical Hopf bifurcation at a larger value of the forward velocity V. However, this is not what we find in the presence of lateral bending. Instead, the stable periodic orbit loses its stability in a torus bifurcation T, which is associated with a second frequency. We find that the torus bifurcation is subcritical and that the solution jumps to stable lateral shimmy oscillations, which are born in the Hopf bifurcation H_l. These lateral oscillations are initially unstable, but stabilize in a torus bifurcation at a velocity V of around 170 m/s. The branch of torsional shimmy oscillations, which is unstable past the point T, disappears in a subcritical Hopf bifurcation at $V \approx 323$ m/s.

Figure 2(b) shows what the one-parameter bifurcation diagram looks like for $F_z = 40.0$ kN. There are several important differences with the case for $F_z = 20.0$ kN. First, the onset of shimmy is now due to a subcritical Hopf bifurcation H at $V \approx 20.5$ m/s. This means that the transition to shimmy is no longer gradual. Instead, the system jumps to large-scale shimmy oscillations past the Hopf bifurcation; this transition is associated with a small hysteresis loop that involves a fold point (saddle-node of limit cycle bifurcation) when V is decreased. Secondly, the nature of the ensuing shimmy oscillations is now quite different. Notice from panel (b2) that the amplitude of the lateral bending stroke δ^* is now substantially smaller, while the torsional component has increased. Thirdly, we find further fold points along the branch of periodic orbits that give rise to more and much larger hysteresis loops. Most pronounced is the hysteresis loop covering the velocity range of $[193, 249]$ m/s. The comparison between Fig. 2(b1) and (b2) shows that this and the smaller hysteresis loop around $V \approx 127$ m/s is characterized by a practically constant amplitude of the torsional component with an increasing (with V) contribution of the lateral bending mode. When stability is lost in the fold point at $V \approx 249$ m/s the system jumps to stable lateral shimmy oscillations (as was the case for $F_z = 20.0$ kN). Finally, we mention that also the second Hopf bifurcation of the (now unstable) branch of torsional shimmy oscillations is now subcritical.

Overall, Fig. 2 provides clear evidence for a significant interaction between the torsional and lateral bending modes of the landing gear. Already for a small vertical force F_z we find torus bifurcations as clear evidence of the interaction of the torsional and the lateral modes. The vertical force F_z has a strong influence on how the behaviour of the nose landing depends on the forward velocity V. In effect, increasing F_z increases the interaction between the two modes. Especially the different hysteresis loops with several stable solutions have serious implications for the aircraft from an operational point of view, because the system may suddenly jump to a different, large-amplitude solution.

3.2 Bifurcation diagram in the (V, F_z)-plane

The bifurcation points that were identified in Fig. 2 can be continued in the (V, F_z)-plane. The result is the two-parameter bifurcation diagram shown in Fig. 3. Its main feature is the interaction between the curve H_t of Hopf bifurcations of the torsional mode and the curve H_l of Hopf bifurcations of the lateral mode.

The torsional Hopf bifurcation curve H_t forms an isola (a closed curve). For lower values of F_z (certainly for $F_z < 30.0$ kN) it corresponds to supercritical Hopf bifurcations leading to shimmy oscillations; compare with Fig. 2(a). In fact, this supercritical part of H_t at low vertical force F_z is as presented in Thota *et al.* [20], where the lateral bending mode was not considered at all. However, the criticality of H_t changes at two degenerate Hopf bifurcation points DH [7,9], so that the

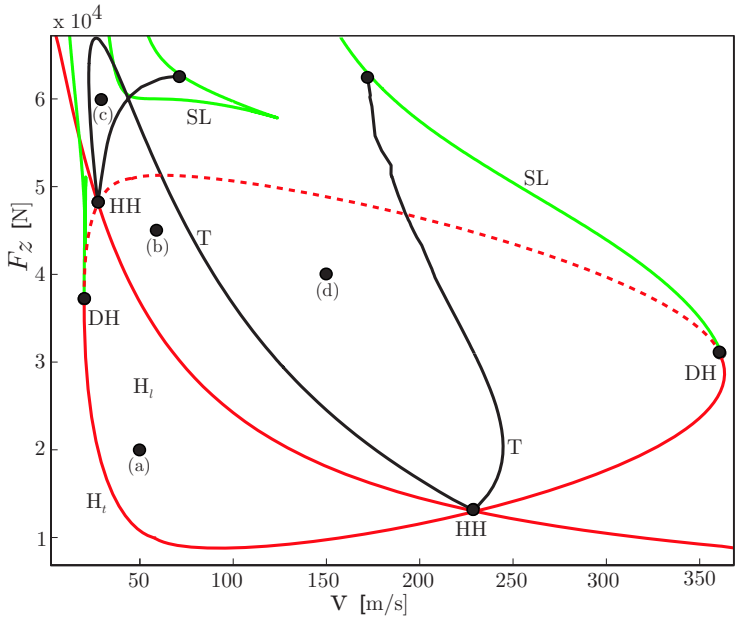

Figure 3 Two-parameter bifurcation diagram of Eqs. (2)–(4) in the (V, F_z)-plane, consisting of curves of Hopf bifurcations (red), saddle-node of limit cycle bifurcations (green) and torus bifurcations (black). The Hopf bifurcation curve H_t of the torsional mode forms an isola and changes criticality at two degenerate Hopf points DH (the dashed part is subcritical); it interacts with the Hopf bifurcation curve H_l of the lateral mode in two double Hopf points HH. For time series of shimmy oscillations for the points labelled (a) to (d) see Fig. 5.

upper part of the isola H_t (in the range 38.0 kN $< F_z <$ 51.0 kN) is subcritical. Hence, it gives rise to unstable shimmy oscillations. Two curves SL of saddle-node of limit cycle bifurcations emerge from the codimension-two points DH, and these can be continued towards larger values of F_z until they exit our region of interest. As a consequence, subcritical Hopf bifurcations for small and large velocity V are preceded and followed by a saddle-node of limit cycle bifurcations; compare with Fig. 2(b).

The lateral Hopf bifurcation curve H_l in Fig. 3 resembles a hyperbola. It intersects the torsional Hopf curve H_t in two Hopf-Hopf bifurcation points HH at ($V \approx 27.6$ m/s, $F_z \approx 48.0$ kN) and ($V \approx 228$ m/s, $F_z \approx 13.0$ kN). We find that two torus curves emerge locally from each of these codimension-two points, which is in agreement with what may be expected from bifurcation theory [7,9]. One of the torus curves connects the two HH points, and the other two can be continued up to curves SL of saddle-node-bifurcations of limit cycles (where they end in 1:1 resonance points [7,9]). Note that the right-most curve T ends on the curve SL that emerges from the right-most point DH on H_t, while the other curve T ends at a separate curve SL. We remark that there are more curves of saddle-node bifurcations of limit cycles that are responsible for the hysteresis loops as in Fig. 2(b). However, they are not shown in Fig. 3 because we focus on the main structure of the bifurcation diagram as it arises from the interaction of H_t and H_l.

Overall, the bifurcation diagram in Fig. 3 provides a global picture of the interaction between the torsional and lateral modes. It is worth mentioning that size and position of the isola H_t, the points DH and emanating curves SL are almost unaffected by changes of the lateral mode (such as its damping). Similarly, changes in the torsional damping or stiffness have very little impact on the Hopf curve H_l.

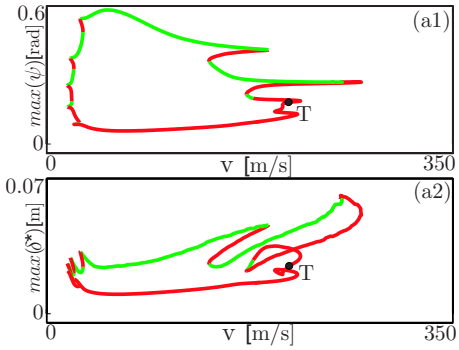

Figure 4 One-parameter continuation in V for $F_z = 55.0$ kN; the top panel shows the maximum of the torsion angle ψ and the bottom panel the maximum of the bending stroke δ^*. Stable parts of branches are green and unstable parts red, with torus bifurcation labelled T.

The basic bifurcation structure is typical for the case that damping and stiffnesses of the torsional and lateral modes are of the same order, in which case the curves H_t and H_l cross in two double Hopf points HH. These codimension-two points act as organising centres of the dynamics in the sense that they give rise to torus bifurcations that lead to quasiperiodic shimmy oscillations. The shape of the torus and Hopf curves suggest that the lateral bending mode may give rise to quasiperiodic shimmy oscillations even at quite low forward velocities, provided that the vertical force is sufficiently large.

An example of the emergence of shimmy for large vertical force is provided by the one-parameter continuation in Fig. 4. Stable shimmy oscillations are born when the left-most curve SL in Fig. 3 is crossed. A number of successive further fold bifurcations (that are not shown in Fig. 3) give rise to small regions of multistability near $V \approx 30.0$ m/s. Considerable regions of multistability and hysteresis can be found in the V-ranges $[140, 191]$ m/s and $[140, 255]$ m/s. As we found before in Fig. 2(b), the amplitude ψ of the lateral mode remains practically constant, while the bending stroke δ^* increases. Note that the shimmy oscillations shown in Fig. 4 are no longer connected to the straight-line motion of the landing gear, because the vertical force of $F_z = 55.0$ kN is above the maximum of the curve H_t. Instead, stable shimmy oscillations appear and disappear suddenly in fold bifurcations.

3.3 Different types of shimmy oscillations

We now present four different types of shimmy oscillations, which we distinguish in terms of the relative contributions of the torsion angle ψ, the bending stroke δ^* and the lateral deformation of the tyre λ_A. Figure 5 shows time series of these quantities for the values of the parameters (V, F_z) corresponding to points (a)–(d) that are labelled in Fig. 3. Just after the onset of shimmy oscillations in the Hopf curve H_t, we find oscillations of the torsion angle ψ at the frequency of the torsional mode; see Fig. 5(a1). These oscillations induce an oscillation of the lateral tyre deformation λ_A. Due to the coupling via the tyre, the lateral stroke follows these oscillations with very small amplitude, but there are no oscillations at the frequency of the lateral mode; see Fig. 5(a2). Hence, this type of dynamics can be characterized as pure torsional shimmy. For sufficiently large vertical force F_z, the influence of the lateral mode is beginning to manifest itself past the Hopf bifurcation curve H_l. While the torsional mode is still dominant [Fig. 5(b1)], the lateral stroke δ^* now shows (faster) oscillations at the lateral mode frequency, which also manifest

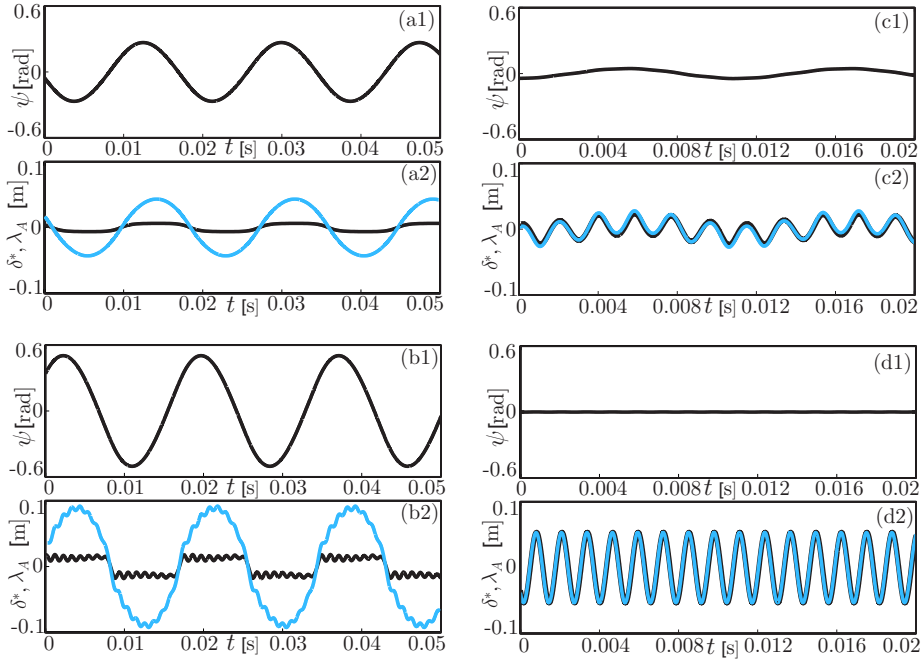

Figure 5 Time series of the torsion angle ψ, and of bending stroke δ^* (black) and lateral tyre deformation λ_A (blue) for the values of (V, F_z) that are labelled (a)–(d) in Fig. 3. Specifically, from (a) to (d) the parameters (V, F_z) take the values (50.0 m/s, 20.0 kN), (60.0 m/s, 45.0 kN), (27.0 m/s, 60.0 kN), and (150 m/s, 40.0 kN), respectively.

themselves in the lateral tyre deformation; see Fig. 5(b2). These dynamics can be characterized as precursory quasiperiodicity. Full-blown quasiperiodic shimmy can be found (for lower values of the forward velocity V) past the left-most torus curve. As panels (c1) and (c2) of Fig. 5 show, both the torsional and the lateral mode are fully excited. This manifests itself via the coupling through the tyre in quasiperiodic in-phase motion of tyre and lateral stroke with the same amplitude. Finally, Fig. 5(d1) and (d2) provides an example of pure lateral shimmy, where only the lateral mode is excited. This type of shimmy is characterized by in-phase oscillations of the lateral stroke δ^* and the lateral tyre deformation λ_A of the same amplitude, while the torsion angle ψ remains practically constant.

4 Discussion and future work

We introduced a mathematical model of an aircraft nose landing gear that takes into account both the torsional and the lateral bending modes of the gear. Both are coupled via the interaction through the tyre, which is modelled by incorporating lateral deformation into the classic stretched string model of von Schlippe. In our model we fully incorporate for the first time the geometric effects of a non-zero rake angle of the landing gear. It manifests itself via several nonlinear coupling effects, which include tilting of the tyre during steering and the generation of an effective caster length. While our model is quite general, we considered here the case of an aircraft landing gear, which is characterized by strong damping of torsional and lateral modes and a moderate rake angle.

The main focus of our study was the interaction of torsional and lateral modes of an aircraft landing gear for realistic values of the different model parameters. In particular, the lateral damping was roughly of the same order as that of the torsional

mode. We presented a bifurcation diagram in the plane of forward velocity V and vertical force F_z as the two main operational parameters. The bifurcation diagram is organised by Hopf bifurcation curves of the torsional and lateral modes, which cross at two double Hopf points. These codimension-two bifurcation points effectively organise the interaction of the two modes by giving rise of torus bifurcation curves that are associated with quasiperiodic shimmy oscillations.

Apart from the well-known torsional shimmy oscillations, we also found stable lateral shimmy and stable quasiperiodic shimmy oscillations to which both the torsional and lateral mode contribute in about equal measure. Shimmy with two frequency components was found in experiments and a 13th-order model of a pulled trailer by Pacejka [11]. More recently, quasiperiodic shimmy has been found by Stépán et al. [15] in a similar experimental setup of a pulled trailer and in a different mathematical model. Importantly, Stépán shows that in the pulled trailer setup the second frequency is due to a delay effect associated with the rolling tyre, which requires a mathematical model in the form of delay differential equations. By contrast, we found that in an aircraft nose landing gear quasiperiodic shimmy may be due simply to the interaction of two different modes of the gear itself. In particular, it is sufficient to model the system by an ordinary differential equation with a phase space of dimension five.

The study performed here shows that the different types of shimmy oscillations can be found in a realistic range of forward velocities, that is, below landing and take-off velocities of between 70 and 100 m/s that are typical for passenger aircraft. From the practical point of view, the influence of the lateral bending mode on the dynamics increases with increasing vertical force on the gear, that is, with loading or braking of the aircraft. Hence, for heavy aircraft one may find pure lateral shimmy or quasiperiodic shimmy instead of more common torsional shimmy oscillations. This may have implications for the design of shimmy dampers for aircraft, which are presently designed to dampen only torsional motion.

There are several directions for future research. First of all, for the landing gear parameters as used in our study, a substantial part of the overall bifurcation structure is beyond the range of realistic velocities. However, preliminary computations have shown that changing certain system parameters, such as the rake angle or the lateral damping rate, results in a shift of the Hopf curves and double Hopf points towards more realistic velocities. A detailed study of the dependence of the bifurcation structure on other parameters is the subject of our ongoing research. Secondly, we mention the evaluation of aircraft taxi, take-off and landing scenarios, which involve specific changes of the vertical force as a function of the forward velocity. The relationship between operational parameters can be determined/calibrated from experimental measurements with the goal of investigating more realistic aircraft operation scenarios. Finally, our landing gear model can be expanded to take into account additional oscillatory modes. In the first instance, this would involve modelling oscillations along the strut axis due to oleo (vertical shock absorber) compression. In the longer term, one may also wish to incorporate dynamical modes that are transmitted by the fuselage. The final goal would be the formulation of an integrated mathematical model of a generic aircraft with all gears, but in such a way that a balance is struck between incorporating the relevant effects while keeping the model amenable to bifurcation analysis.

5 Acknowledgments

We thank Hans Pacejka for helpful comments on how to introduce the lateral deformation into the tyre model, and Robert Szalai for his help with the two-parameter continuation of torus bifurcations. This research has been supported by Airbus.

References

1. Baumann, J.: A Nonlinear model for landing gear shimmy with applications to the McDonnell Douglas G/A-18A. 81^{st} Meeting of the AGARD Structures and Materials Panel, (1995).
2. Besselink, I. J. M.: Shimmy of aircraft main landing gears. Dissertation, University of Delft, The Netherlands, (2000).
3. Broulhiet, M. G.: La suspension de la direction de la voiture automobile - Shimmy et dandinement. Bull. Soc. Ing. Civ.(France), 78, (1925).
4. Dengler, M., Goland, M. and Herrman, G.: A bibliographic survey of automobile and aircraft wheel shimmy. Technical report, Midwest Research Institute, Kansas city, MO, USA, (1951).
5. Doedel, E. J., Keller, H. B. and J. P, Kernevez, J.P.: Numerical analysis and control of bifurcation problems, Part II : Bifurcation in infinite dimensions. J. Bifur. Chaos Appl. Sci. Engrg. 1(4), 745–772(1991).
6. Glaser, J. and Hrycko, G.: Landing gear shimmy - De Havilland's experience. 81^{st} Meeting of the AGARD Structures and Materials Panel, (1995).
7. Guckenheimer, J. and Holmes, P.: Nonlinear oscillations, dynamical systems and bifurcations of vector fields. Springer, New York (1983).
8. Krabacher, W. E.: A Review of Aircraft Landing Gear Dynamics. 81^{st} Meeting of the AGARD Structures and Materials Panel, (1995).
9. Kuznetsov, Y. A.: Elements of applied bifurcation theory. Springer, New York (1995).
10. Pacejka, H. B.: Analysis of the shimmy phenomenon. Proceedings of The Institute of Mechanical Engineers. 180(2A)(10), (1965-66).
11. Pacejka, H. B.: The wheel shimmy phenomenon: A theoretical and experimental investigation with particular reference to the nonlinear problem. Dissertation, Delft University of Technology, (1966).
12. Pritchard, I. J., An overview of landing gear dynamics. NASA Technical Reports, NASA/TM-1999-209143, (1999).
13. Smiley, R. F.: Correlation, evaluation, and extension of linearized theories for tyre motion and wheel shimmy. Report submitted to the National Advisory Committee for Aeronautics, Report 1299, (1957).
14. Somieski, G.: Shimmy analysis of a simple aircraft nose landing gear model using different mathematical methods. Aerosp. Sci. Technol. 1270-9638(8), (1997).
15. Stépán, G.: Delay, Nonlinear Oscillations and Shimmying Wheels. Kluwer, Dordrecht (1998).
16. Stépán, G.: Chaotic motion of wheels. Vehicle Syst Dyn. 20(6), 341–351(1991).
17. von Schlippe, B. and Dietrich, R.: Shimmying of a pneumatic wheel. Report submitted to the National Advisory Committee for Aeronautics, NACA TM 1365, (1947).
18. Takacs, D. and Stépán, G.: Experiments on quasi-periodic wheel shimmy. Proc. IDETC/CIE. DETC2007-35336, (2007).
19. Takacs, D., Stépán, G. and Hogan, J. H.: Isolated large amplitude periodic motions of towed rigid wheels. Nonlinear Dynam. 52(1-2), 27–34(2007).
20. Thota, P., Krauskopf, B. and Lowenberg, M.: Shimmy in a nonlinear model of an aircraft nose landing gear with non-zero rake angle. Proceedings of ENOC, (2008).
21. Woerner, P. and Noel, O.: Influence of nonlinearity on the shimmy behaviour of landing gear. 81^{st} Meeting of the AGARD Structures and Materials Panel, (1995).